RiceTalk: Rice Blast Detection Using Internet of Things and Artificial Intelligence Technologies

Wen-Liang Chen, Yi-Bing Lin, *Fellow, IEEE*, Fung-Ling Ng, Chun-You Liu, and Yun-Wei Lin

***Abstract*—Rice blast is one of the most serious plant diseases. Many rice blast management approaches require know-how of experienced farmers or agronomists. Monitoring the farm for disease detection is labor intensive and time consuming. By using the Internet of Things (IoT) and artificial intelligence (AI), we are able to detect plant diseases more efficiently. Existing AI and IoT studies detect plant diseases by images or nonimage hyperspectral data, which require manual operations to obtain the photographs or data for analysis. Also, image detection typically is too late as rice blast may already spread to other plants. Based on an IoT platform for soil cultivation, we develop the RiceTalk project that utilizes nonimage IoT devices to detect rice blast. Unlike the image-based plant disease detection approaches, our agriculture sensors generate nonimage data that can be automatically trained and analyzed by the AI mechanism in real time. The beauty of RiceTalk is that the AI model is treated as an IoT device and is managed like other IoT devices. In this way, our approach significantly reduces the platform management cost to provide real-time training and predictions. We also propose an innovative spore germination mechanism as a new feature extraction model for agriculture. In the current implementation, the accuracy of the RiceTalk prediction on rice blast is 89.4%.**

***Index Terms*—Artificial intelligence (AI), precision farming, rice blast, soil cultivation, spore germination.**

I. Introduction

MAHATMA Gandhi (1869–1948) said: "If you give me rice, I'll eat today; if you teach me how to grow rice, I'll eat every day." Rice is considered as a staple food for hundreds of millions of people in the world today. Rice crop failures potentially cause starvation. A major reason for rice crop failure is the attack of rice blast that is one of the most serious plant diseases [1], [2]. The fungus causing rice blast is *Magnaporthe oryzae* (or *Magnaporthe grisea*), which results in lesions on leaves (Fig. 1), stems, peduncles, panicles, seeds, and roots. For the first cultivation of a year in Taiwan, rice blast disease typically spreads over one-tenth of the total cultivated area in the rice crop.

Fig. 1. Rice blast in paddy fields (by courtesy of Taichung District Agricultural Research and Extension Station, COA, Taiwan).

Many rice blast management approaches have been proposed, but often with limited success due to the fact that detecting rice blast requires know-how of experienced farmers or agronomists, and monitoring the farm for disease detection is labor intensive and time consuming [3]. Due to technological advances in the Internet of Things (IoT) and artificial intelligence (AI), we are able to detect plant diseases more efficiently. In [4], the spot color features on the plant parts are analyzed by image processing for grape disease recognition with 90% accuracy from 100 photographs. The number of photographs used in this article is small, and the results should be further investigated. In [5], digital plant disease detection was developed based on a deep convolutional neural network (CNN) to classify three types of diseases and two types of pests for cassava leaves with an overall accuracy of 93%. In [6], a multidisease identification algorithm was proposed to classify rust, septoria, and tan spot diseases from wheat images. Color constancy algorithms were used to reduce natural illumination variability effects resulting in about 80% accuracy. In [7], the advanced neural network techniques for processing hyperspectral data are surveyed for plant disease detection. The above studies detect plant diseases by images or nonimage hyperspectral data, which require manual operations to obtain the photographs or data for analysis for the following reason. Since the sizes of rice fields are large, it is impossible to deploy multiple cameras and hyperspectral sensors of a wired or wireless sensor network in a huge rice field (to the best of our knowledge, no one takes this approach due to cost consideration). It is also impossible to use drones to

Manuscript received April 8, 2019; revised May 23, 2019 and August 20, 2019; accepted October 6, 2019. Date of publication October 16, 2019; date of current version February 11, 2020. This work was supported in part by the Ministry of Science and Technology under Grant 106N490, Grant 107R491, and Grant 108-2221-E-009-047; and in part by the Center for Open Intelligent Connectivity from the Featured Areas Research Center Program Within the Framework of the Higher Education Sprout Project by the Ministry of Education in Taiwan. *(Corresponding author: Yi-Bing Lin.)*

W.-L. Chen and F.-L. Ng are with the College of Biological Science and Technology, National Chiao Tung University, Hsinchu 30050, Taiwan (e-mail: wenurea@gmail.com; ngfungling9@gmail.com).

Y.-B. Lin and C.-Y. Liu are with the Department of Computer Science, National Chiao Tung University, Hsinchu 30050, Taiwan (e-mail: liny@nctu.edu.tw; chunyou@ itri.org.tw).

Y.-W. Lin is with the College of Artificial Intelligence, National Chiao Tung University, Hsinchu 30050, Taiwan (e-mail: jyneda@gmail.com).

Digital Object Identifier 10.1109/JIOT.2019.2947624

detect rice blast because the cameras in the air cannot detect early rice blast infection in the leaves near the roots. Therefore, to the best of our knowledge, all image or hyperspectral-based approaches require the farmer to manually carry a smartphone or a handheld device to take pictures or other actions. The farmer can only periodically take the photographs, therefore, the tedious labor and the detection delay are very serious problems. Furthermore, such image detection typically is too late as rice blast may already spread to other plants.

Katsantonis *et al.* [10] surveyed 52 studies that detect rice blast using nonimage sensors. The survey concluded that these studies have low applications due to inaccuracies and uncertainties in the predictions. The survey also indicated that an important factor "spore germination" is not used in these studies. Based on AgriTalk [8], an IoT platform for soil cultivation, we develop the RiceTalk application that utilizes nonimage IoT devices, including the weather station and the soil sensors for precision monitoring, and the cultivation actuators for irrigation, pest control, and fertilization. Unlike the image-based plant disease detection approaches, AgriTalk sensors generate nonimage data that can be automatically trained and analyzed by the AI mechanism in real time. The beauty of AgriTalk is that the AI model is treated as an IoT device and can be managed like other IoT devices (i.e., the agriculture sensors and actuators), which nicely integrates the IoT and the AI mechanisms. We further propose a spore germination model as a feature to machine learning, which has not been found in the literature. From the view point of AI, this spore germination mechanism is an innovative feature extraction model for agriculture.

This article shows how RiceTalk effectively detects rice blast disease. This article is organized as follows. Section II gives an overview to rice blast. Section III elaborates on the RiceTalk project. Section IV describes the data extraction and AI intelligence implemented in RiceTalk. Section V investigates the prediction accuracy of RiceTalk.

II. Overview to Rice Blast

The most common sign of rice blast is diamond-shaped lesions occurring on the leaves [9]. The leaf lesions initially appear as the small gray-green spots, and then become yellowish brown and withered. If the collar of a rice plant (the junction of the leaf and the stem sheath) is infected, the entire leaf could be compromised, and the fungus may produce spores on such lesions. Infection of the neck (the portion of the stem that grows above the leaves to support the panicle) results in seed filling (also known as blanking) failures and entire panicle falling over as if rotted. The lesions are dark brown at the beginning, then black. The branches become dry, shrink, sag, and are easy to break. In the blanking condition, the pedicels are infected and the plants cannot produce seeds. The farmers or any smart solution based on image processing can detect rice blast visually through the above symptoms. However, such visual (image) detection typically is too late as rice blast may already spread to other plants.

Without the need of image examination, AgriTalk utilizes nonimage sensors to detect the environmental conditions that may cause rice blast. With high humidity and moderate warm temperature ranging from 20 °C to 32 °C, the fungus sporulates on seed lesions and in the center of the lesions on susceptible cultivars. These spores called conidia are produced abundantly on infected leaf, collar, panicle, and seed through specialized stalks called conidiophores that extend beyond lesion surfaces. About 80% of conidia germinate within 3 h. Infection of rice occurs when conidia are left on rice tissues and germinate in warm climates (e.g., the temperature ranges from 12 °C to 36 °C). An infection peg is developed from the appressorium to penetrate the tissue when temperature ranges from 15 °C to 25 °C. A minimum dew period of 6–8 h will initiate infection at the optimum temperature of 25 °C [10]. After penetration, the primary infection hypha grows rapidly (in 6 h), and branches within vulnerable tissues for 2 or 3 days to form conidiophores. After conidiophores have grown for 4 h, they start to produce the spores. The spores mature after 50–90 min, and leave the conidiophores as the second source of infection in the crop field. In this way, rice blast disease spreads quickly in the crop field. Sporulation potential is higher at 20 °C and infection may continue in the subsequent plantings of the crop field because the disease sources in the previous planting may invade seeds on the soil surface after the next planting to produce more spores of *P. oryzae* within several weeks. For example, after planting in Arkansas, the first lesions are observed in 45–55 days. After infection, the secondary lesions appear within a few days to produce more spores that are spread to nearby leaves by wind. Such an infection process may repeat several times depending on the level of genetic resistance in the infected cultivar, the temperature, rainfall, and the amount of nitrogen in fertilizers [11]–[13]. The above studies indicate that mature lesions have a high rate of conidia producing when relative humidity is greater than 89%. If leaf wetness ends before the completion of infection, the process is terminated. Increasing the leaf wetness period from 12 to 15 h is known to result in a 30% increase in infection. The shortest period of leaf wetness needed for successful infection is 12 h, within a temperature range of 20 °C–25 °C. Germination commonly begins within 3 h of deposition if leaves are wet. Inhibition increases with an increase in the duration of exposure to sunlight. Inhibition was slightly more in case of wet spores.

Several rice blast management approaches have been proposed. Crop rotation effectively separates sustainable spores in harvest residue from the newly developing seedlings [14]. However, the crop field cannot be reused in a short period of time. Crop rotation can be avoided if precision farming technique, such as RiceTalk (to be elaborated in this article) is exercised to prevent rice blast infection in the previous planting. Proper fertilization decreases the amount of rice blast in the fields and significantly increases yields [15]. Proper fertilization can also be achieved by AgriTalk's precision irrigation and fertilization system as described in [8]. A last resort for rice blast is the use of chemical fungicides to control the disease. Seedling infection can be prevented by the seed treatment of fungicides. On the other

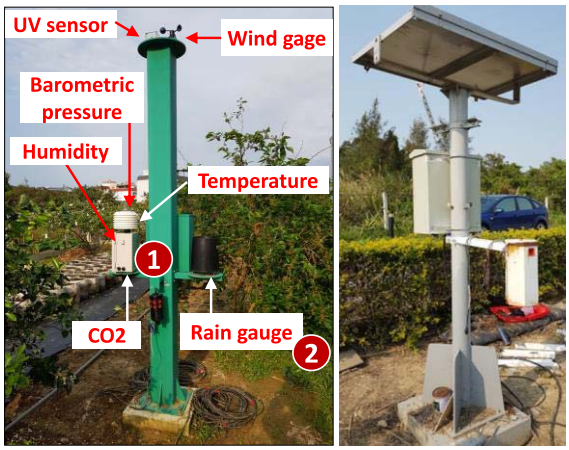

Fig. 2. Two AgriTalk micro weather stations.

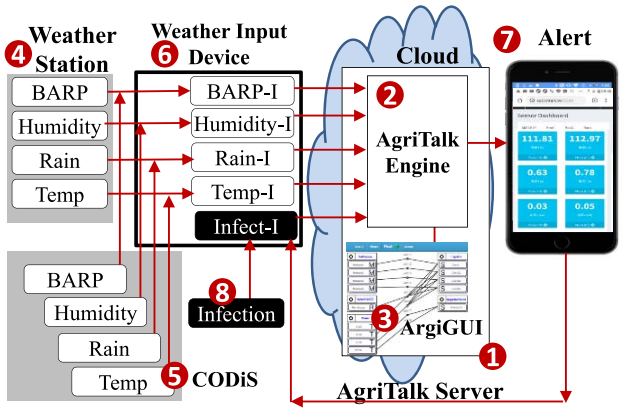

Fig. 3. AgriTalk architecture for the RiceTalk application (the IoT part).

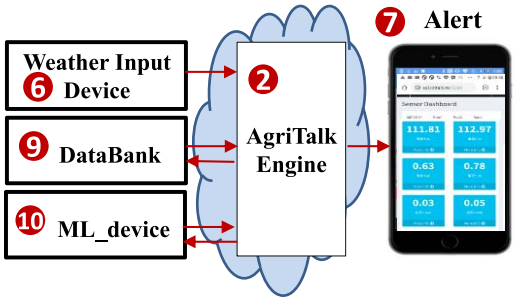

Fig. 4. AgriTalk architecture for the RiceTalk application (the AI part).

hand, rice blast on the panicles can be reduced by applying fungicides to the foliage once or twice to protect the panicles when they are emerging from the boot.

III. RiceTalk Application Configuration

Based on AgriTalk [8], this article develops the RiceTalk application. This application utilizes the weather data obtained from the Observation Data Inquire System (CODiS) of Central Weather Bureau in Taiwan [16] and the real-time data of the AgriTalk sensors from the micro weather stations we established in four locations. Fig. 2 illustrates two weather stations of AgriTalk. In every station, the temperature, the relative humidity, and the barometric pressure sensors [Fig. 2(1)] and the rain gauge [Fig. 2(2)] are used in the RiceTalk application.

Figs. 3 and 4 illustrate the AgriTalk architecture for the RiceTalk application. The AgriTalk server [Fig. 3(1)] consists of the AgriTalk Engine [Fig. 3(2)] and the AgriTalk graphical user interface called AgriGUI [Fig. 3(3)]. The AgriTalk Engine receives the sensor data from the AgriTalk weather station [Fig. 3(4)] and the CODiS data from the Central Weather Bureau [Fig. 3(5)] through a software module called "Weather input device" [Fig. 3(6)]. The input data are processed at the engine and then the results are sent to a Web-based alert dashboard that can be accessed from a computer or a smartphone [Fig. 3(7)]. Besides the sensor data, there is a special input connected to the Weather input device called "Infection." This input is used for labeling of AI model training. The historical data for the features come from CODiS [Fig. 3(5)] and the corresponding labels (to indicate whether rice blasts occur or not) come from the Bureau of Animal and Plant Health Inspection and Quarantine [Fig. 3(8)]. The AgriTalk weather stations provide real-time AI features [Fig. 3(4)]. In the training phase, an experienced farmer may also check if rice blast occurs. The farmer then sends the result (the label value) through the smartphone [Fig. 3(7)] to the Weather input device.

The beauty of AgriTalk is that the AI model is treated as an IoT device and is managed like other IoT devices (i.e., the agriculture sensors and actuators). This approach significantly reduces the platform management cost to provide real-time training and prediction. The AI configuration part of AgriTalk is illustrated in Fig. 4, where two cyber devices are connected to AgriTalk engine. The DataBank cyber device [Fig. 4(9)] preprocesses the data received from the Weather input device [Fig. 4(6)], and the ML_device cyber device [Fig. 4(10)] executes the AI model to produce the prediction results sent to the Alert device [Fig. 4(7)].

AgriGUI allows the user to create an IoT project by manipulating the icons in the GUI window as described in [8]. Through the GUI window, we develop the project with the name RiceTalk. The sensors or controls of an IoT device [e.g., Fig. 3(6)] are grouped in an icon called "input device." The actuators of an IoT device [e.g., Fig. 3(7)] are grouped in an icon called "output device."

In the RiceTalk project, we create two cyber devices DataBank and ML_device [Fig. 4(9) and (10)] that have both input and output parts. The output device of DataBank receives the weather information as the inputs (which are appended with "-I" to represent "inputs"), and manipulates the data to extract their characteristics, such as the average, the minimum, and the maximum of the samples. The extracted weather data are sent out through the DataBank input device. Details of DataBank will be given in Section IV-A. ML_device is an AI machine implemented as an IoT device through the novel idea described in [17]. The setup for RiceTalk AI model is given in Section IV-C. The values received by the output device of ML_device [Fig. 4(10)] are run on a powerful AI machine to conduct real-time machine learning. The advantage of implementing ML_device as an IoT device is that it can utilize various AI tools (e.g., tensorflow in our example)

Fig. 5. AgriTalk dashboard.

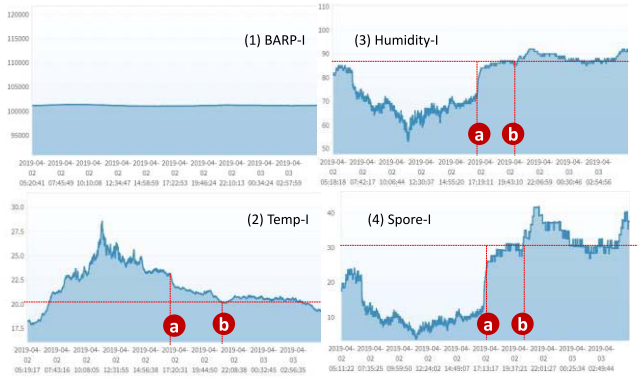

Fig. 6. Time series for BARP-I, Humidity-I, Temp-I, and Spore-I.

executed on a powerful machine that is automatically connected to the AgriTalk server. The prediction results are then sent to the Alert device [Fig. 4(7)] from the input device of ML_device.

AgriTalk implements the Alert device as a Web-based dashboard that gives real-time measures of the sensors, which can be easily accessed in an arbitrary smartphone. The dashboard includes the barometric pressure icon BARP-I [Fig. 5(1)], the temperature icon Temp-I [Fig. 5(2)], the relative humidity icon Humidity-I [Fig. 5(3)], and the spore germination rate icon Spore-I [Fig. 5(4)]. When a sensor icon is clicked, the time series chart for that sensor is shown in Fig. 6. We will elaborate more on Fig. 6 later.

IV. Data Extraction and AI Intelligence

In RiceTalk, the raw data are processed at DataBank to extract the features we want to feed to the AI model. Section IV-A describes the measures (the features of the AI model) that can be produced in DataBank. Section IV-B shows how spore germination prediction is implemented. Section IV-C elaborates on the construction of ML_device as the AI model for rice blast prediction.

A. Raw Data Extraction

We have collected the data from the Central Weather Bureau [Fig. 3(5)] and the Bureau of Animal and Plant Health Inspection and Quarantine [Fig. 3(8)] since 2011. The AgriTalk data [Fig. 3(4)] have been collected since 2018. As illustrated in Fig. 3(6), we use the following environment conditions (data produced by the sensors) in the current RiceTalk implementation:

$$\boldsymbol{S} = \{B, T, R, H, S\}$$

where B is BARP-I, T is Temp-I, R is Rain-I (obtained from the rain gauge), H is Humidity-I, and S is Spore-I. Note that Spore-I is derived from Temp-I and Humidity-I to be described in Section IV-B.

We collected the raw data of a sensor $s \in \boldsymbol{S}$ in $J = 2738$ observation days, and these observation days are partitioned into $J - I + 1$ periods. Every period has I days, and the next period shifts one day toward the present day as compared to the previous period. Suppose that we collect N samples for sensor s in the ith day of a period (where $1 \le i \le I$); then the sample set $\boldsymbol{E}_{s,i}$ is

$$\boldsymbol{E}_{s,i} = \left\{e_{s,i,1}e_{s,i,2}, \ldots, \ldots e_{s,i,n}, \ldots, e_{s,i,N}\right\}.$$

In our experiments, $N = 24$. From every observation day, DataBank extracts the following measures from the data set $\boldsymbol{E}_{s,i}$. For BARP-I, Temp-I, Humidity-I, and Spore-I (that is, $s \in \{B, T, H, S\}$), the measures are as follows.

1) The minimum measure $x_{m,s,i} = \min_{e_{s,i,n} \in \boldsymbol{E}_{s,i}} e_{s,i,n}$.
2) The maximum measure $x_{M,s,i} = \max_{e_{s,i,n} \in \boldsymbol{E}_{s,i}} e_{s,i,n}$.
3) The average measure $x_{a,s,i} = (e_{s,i,1} + e_{s,i,2} + \cdots + e_{s,i,n} + \cdots + e_{s,i,N})/N$.
4) The range measure in a day $x_{r,s,i} = x_{M,s,i} - x_{m,s,i}$.
5) The daily difference measure [the difference of the averages between the ith day and the (i–1)th day] $x_{d,s,i} = |x_{a,s,i} - x_{a,s,i-1}|$.

For Rain-I, two measures are defined.

1) The accumulated amount measure $x_{a,R,i}$ of rainfall in the ith day.
2) The daily difference measure $x_{d,R,i} = |x_{a,R,i} - x_{a,R,i-1}|$.

For $z \in \{a, m, M, r, d\}$ and $s \in \boldsymbol{S}$, we define

$$\boldsymbol{x}_{z,s,I} = \left\{x_{z,s,i} | 1 \le i \le I\right\}.$$

Therefore, for any sensor $s \in \{B, T, H, S\}$, the measure set of s is

$$\boldsymbol{x}_{s,I} = \left\{\boldsymbol{x}_{z,s,I} | z \in \{a, m, M, r, d\}\right\} \tag{1}$$

and

$$\boldsymbol{x}_{R,I} = \left\{\boldsymbol{x}_{a,R,I}, \boldsymbol{x}_{d,R,I}\right\}. \tag{2}$$

From (1) and (2), the measure space in this article is

$$\boldsymbol{x}_I = \{\boldsymbol{x}_{s,I} | s \in \boldsymbol{S}\}. \tag{3}$$

The RiceTalk designer can select appropriate measures from the set $\boldsymbol{x}_I$ and use them as the features to be processed in the AI model.

It is clear that these measures attempt to catch the characteristics of the time series for the sensor. For example, the $\boldsymbol{x}_{d,s,I}$ measure provides the relationship of the sensor data between the ith and $(i-1)$th days. Both $\boldsymbol{x}_{r,s,I}$ and the $(\boldsymbol{x}_{m,s,I}, \boldsymbol{x}_{M,s,I})$ pair provide similar information, but have different effects to be described in Section V.

(a) (b)

Fig. 7. Two spore states observed under the microscope. (a) No spore germination. (b) Spore germination.

B. Spore Germination Function

Temperature and relative humidity are two important environmental parameters that affect spore germination rate in the rice field. Therefore, these two parameters are used to build a general model of germination rate [18]. In the beginning, we analyzed the data from the previous studies that have shown various fungi spore germination rates under different temperature and humidity conditions [19], [20]. The types of fungi include *Myce-liophthora thermophila*, *Aspergillus niger*, *P. oryzae*, *Diplodia corticola*, and *Pseudocercospora*. Based on the above studies, we designed the spore germination rate function [21]. Specifically, we defined how the interaction of temperature and relative humidity affects spore germination. The spore germination rate function $f_T(z)$ based on temperature is a cubic equation

$$f_T(z) = a_T z^3 + b_T z^2 + c_T z + d.$$

We also define the spore germination rate $f_H(z)$ based on relative humidity with a nonlinear equation

$$f_H(z) = a_H \times \exp(b_H z).$$

The coefficients in the above equations are obtained through biological experiments on the spores with various temperature and relative humidity values. In these experiments, we observed spore germination rates with the microscope. Fig. 7 shows the two states of spore: 1) no germination and 2) germination.

Based on the observed interaction of temperature and relative humidity, we determined the coefficients for the spore germination rate function through curve fitting. For temperature $e_{T,i,n} \in \boldsymbol{E}_{T,i}$ (in °C) and relative humidity $e_{H,i,n} \in \boldsymbol{E}_{H,i}$ (in %), the results are

$$f_T(e_{T,i,n}) = -0.0078 e^3{}_{T,i,n} + 0.2806 e^2{}_{T,i,n} + 1.6665 e_{T,i,n} + 0.27 \quad (4)$$

$$f_H(z_{H,i,n}) = 0.1143 \times \exp(6.6027 e_{H,i,n}). \quad (5)$$

Assume that temperature and humidity are independent measures, the general fungal spore germination model f_G can be obtained by multiplying (4) and (5)

$$f_G(e_{T,i,n}, e_{H,i,n}) = f_T(e_{T,i,n}) \times f_H(e_{H,i,n}). \quad (6)$$

Our model was validated by comparing the predicted germination rate with the results of spore germination experiments. The experiments showed that, for example, at high temperature (e.g., 23 °C) and high relative humidity (e.g., 97%), the spore germination rate obtained from the measurements is 92.45%, while the prediction result is 86.84%. At low temperature (e.g., 13 °C) and relative low relative humidity (e.g., 80%), the spore germination rate obtained from measurement is 5.41%, while the prediction results 6.84%. The f_G function (6) is implemented in the RiceTalk through the Join connection. Details of the Join mechanism can be found in [8].

Fig. 6 shows the time series for BARP-I, Humidity-I, Temp-I, and the resulting Spore-I for April 2, 2019, which are measured by the AgriTalk micro station at the Bao field in Hsinchu. Note that the values of Spore-I are computed in real time in AgriTalk. The figure indicates that the temperature drops from 23.5 °C at April 2, 17:13 [point (a)] to 20 °C at April 2, 20:00 [point (b)]. In the same period, the relative humidity increases from 70% to 89%, and the predicted spore rate increases from 25% to 30%. After point (a), the temperature is stable at 20 °C, and relative humidity continues to slightly increase, which result in increasing spore germination rate. The prediction of (6) is consistent with the previous studies mentioned in Section II, that is, sporulation potential is higher at 20 °C, and mature lesions have high rate of conidia producing when relative humidity is greater than 89%.

C. AI Model

For $\boldsymbol{x}_I^* \in \boldsymbol{X}_I$, let $p(\boldsymbol{x}_I^*)$ be the accuracy probability of positive prediction for detecting rice blast by executing the AI model. That is, $p(\boldsymbol{x}_I^*)$ is the probability that rice blast occurs in the Ith day and RiceTalk predicts that rice blast occurs. Define the accuracy probability of negative prediction $\overline{p}(\boldsymbol{x}_I^*)$ as the probability that rice blast does not occur in the Ith day and RiceTalk predicts that rice blast does not occur. It is clear that $p(\boldsymbol{x}_I^*)$ should be large so that the farmer can detect rice blast most of the times, and $\overline{p}(\boldsymbol{x}_I^*)$ should be large so that the farmer only receives few false alarms. The net accuracy probability of both positive and negative predictions is denoted as $P(\boldsymbol{x}_I^*)$. Among $J = 2738$ days in our experiment, 5267 samples were made in 158 locations for the labeling of rice blast status. The sampling survey reported how many areas are infected in percentage. The average areas of infection are 4.1%, and the standard deviation is 10.8%. This article labels the sampling of an area as infected if more than 0% of the area is infected. According to the survey, rice blast occurred in 17.4 days per location, and there are 2747 rice blast events among 5267 samplings.

Rice blast infection is influenced by the change of weather as well as spore germination. This relationship is difficult to recognize by humans, but can be captured by an AI model. In our AI model, the number of features is $|\boldsymbol{x}_I^*|$. These features are represented by a 2-D array whose size is the number of the measures times I days. The label consists of two classes: 1) negative (rice blast does not occur) and 2) positive (rice blast does occur). To simplify our discussion, we assume that the number of measures is 5 in Fig. 8. In real scenarios, the number of measures is larger than 10.

RiceTalk utilizes CNN [24], a powerful tool to automatically recognize the feature patterns over a period of time. We have considered other AI models, including KNN, SVM,

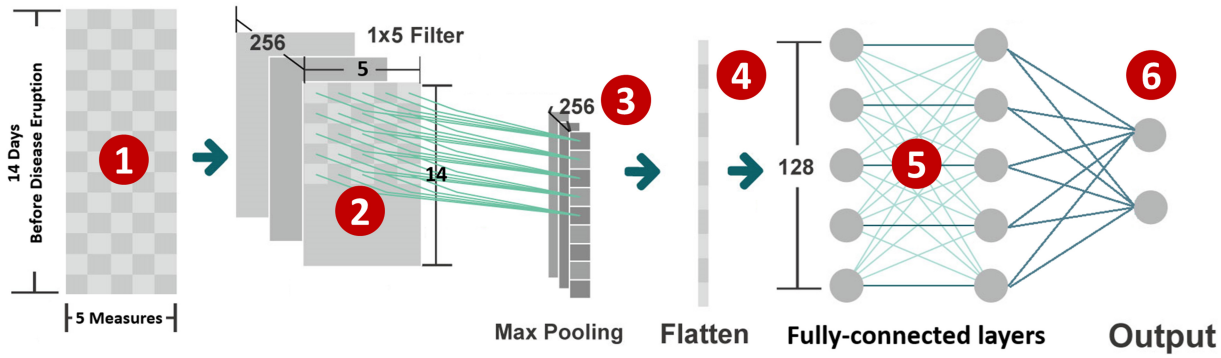

Fig. 8. CNN model used in RiceTalk.

decision trees, and random forests [17]. The rice blast detection accuracies of these AI models are not as good as CNN. CNN perfectly fits rice blast detection because it can model the favorite weather change to the fungal diseases in the life cycle. Consider $\boldsymbol{x}_I^*$ with five measures in 14 days [Fig. 8(1)] as the 14×5 features to the first convolutional layer. This layer [Fig. 8(2)] filters the 14×5 input features with 256 kernels of size 5×1, i.e., each kernel considers 1 measure and 5 days at a time. The layer slides every kernel with a stride of size 2×1 at a time. In Fig. 8(3), a max-pooling layer is used to filter some noises, which only returns the maximum values. This action does not remove useful information because weather patterns that cause diseases will not change in a short period of time. At this layer, the weather features are converted to weather change features. Note that the max-pooling output is a 2-D tensor, which is flattened to four 1-D vectors in Fig. 8(4). The vectors are fed to four fully connected layers [Fig. 8(5)], where every layer has 128 neurons. We use dropout (i.e., the output of each hidden neuron is set to 0 with probability 0.5) in all fully connected layers. The "dropped out" neurons do not participate in either forward pass or backpropagation in training [25]. In this way, more robust models will be learned in conjunction with many different random subsets of neurons. Then, the resulting vector of size 128 is sent to the output layer [Fig. 8(6)]. This layer has two neurons representing how negative and how positive of the result, and their outputs are normalized by the softmax function. This classified result is compared with the label to produce the accuracy probabilities $P(\boldsymbol{x}_I^*)$, $\overline{p}(\boldsymbol{x}_I^*)$, and $p(\boldsymbol{x}_I^*)$. To speed up the training process, the rectified linear units (ReLUs) are applied to the output of the convolutional layer and every fully connected layer. In our approach, the parameters of the neural network are optimized by Adam optimizer [22].

The above RiceTalk AI model is implemented by configuring ML_device [17]. This AI model is built through the detailed setup by the ML setup window illustrated in Fig. 9.

Feature Extraction: In Fig. 9(1), one-stage feature extraction is used, which is set up by selecting the stage number "1." Five measures of 14 days are created as five vectors of size 14 in stage 0, which are the inputs of stage 1. stage 1 is a 5×5 matrix, where the diagonal elements are checked to represent that vector i of stage 0 is connected to vector i of stage 1 (where $1 \leq i \leq 5$). In this matrix, the data for different sensors are standardized.

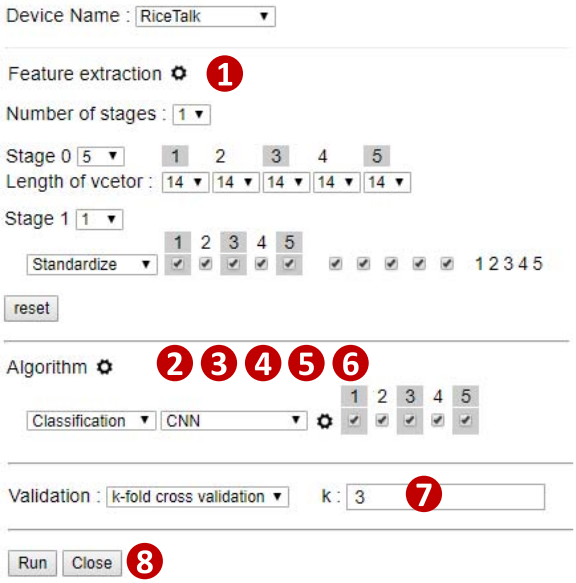

Fig. 9. Setup of the AI model.

Algorithm Selection: The CNN algorithm is selected and configured as illustrated in Fig. 9(2)–(6). The details can be found in [17], and are not repeated here.

Validation: In Fig. 9(7), the k-fold method is used for cross-validation where $k = 3$.

Model Training: When we click the "Run" button [Fig. 9(8)], RiceTalk starts collecting data and training the model. The historical data or real-time data are sent to ML_device for execution. Through k-fold cross-validation, we obtain three prediction probabilities.

V. Performance Evaluation

This section investigates the accuracy performance of RiceTalk. The prediction accuracies are affected by both the sensor measures (from DataBank) and the hyperparameters of

TABLE I
EFFECTS OF SENSOR MEASURES WHERE THE PROBABILITIES AND IMPROVEMENTS ARE GIVEN IN % ($I = 14$)

Scenario	1	2	3	4	5	6	7	8	9	10	11	12	13	14	15	16	17	18	19
s	ϕ	B	B	B	B	H	H	H	H	R	R	T	T	T	T	S	S	S	S
z	ϕ	a	m/M	r	d	a	m/M	r	d	a	d	a	m/M	r	d	a	m/M	r	d
$P_{z,s}$	85.7	85.4	85.9	85.7	85.5	86.1	85.1	85.5	85.6	85.9	85.7	85.5	85.4	86.4	85.5	85.6	86.1	86.0	85.4
$\upsilon_P(z,s)$	0.0	0.3	-0.3	-0.1	0.3	-0.5	0.7	0.2	0.1	-0.2	-0.1	0.2	0.3	-0.9	0.3	0.1	-0.5	-0.3	0.3
$\overline{p}_{z,s}$	82.3	83.4	84.0	83.3	82.1	83.0	83.2	83.9	82.4	83.4	83.7	83.7	82.7	84.6	81.8	82.4	83.7	84.1	82.9
$\upsilon_{\overline{p}}(z,s)$	0.0	-1.3	-2.0	-1.2	0.3	-0.9	-1.0	-1.9	-0.1	-1.3	-1.6	-1.6	-0.4	-2.7	0.6	-0.1	-1.6	-2.2	-0.7
$p_{z,s}$	88.6	87.1	87.6	87.9	88.4	88.8	86.7	86.9	88.4	88.0	87.6	87.1	87.8	88.0	88.6	88.3	88.3	87.6	87.6
$\upsilon_p(z,s)$	0.0	1.7	1.2	0.8	0.2	-0.2	2.2	2.0	0.2	0.7	1.2	1.7	1.0	0.7	0.0	0.4	0.4	1.2	1.2

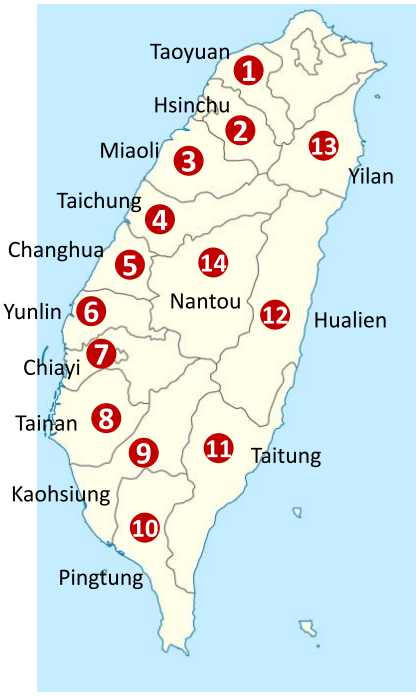

Fig. 10. Fourteen counties of Taiwan investigated in this article.

the CNN model (from ML_device). The optimal hyperparameter setups are presented in Section IV-C after tedious testing and tuning. The details are omitted.

We have obtained the weather data for 158 locations in 14 counties in Taiwan. Let $\boldsymbol{C}$ be the set of the counties, specifically, $\boldsymbol{C}$ = {Taoyuan, Hsinchu, Miaoli, Taichung, Changhua, Yunlin, Chiayi, Tainan, Kaohsiung, Pingtung, Taitung, Hualien, Yilan, Nantou}. Fig. 10 shows the locations of these counties numbered in the order of the elements listed in $\boldsymbol{C}$. In [21], we used $\boldsymbol{x}_I^* = \boldsymbol{x}_I - \boldsymbol{x}_{S,I}$, i.e., without considering the Spore-I measures, and obtained $P(\boldsymbol{x}_I^*) = 82.5\%$. We will show that Spore-I measures significantly improve the rice blast prediction accuracy from 82.5% to 87.2%.

A. Effects of Sensor Measures

Let $\boldsymbol{x}_I(c)$ be a subset set of $\boldsymbol{x}_I$ given in (3), which represents the weather data collected from county $c \in \boldsymbol{C}$. That is, $\boldsymbol{x}_I = \{\boldsymbol{x}_I(c) |\ c \in \boldsymbol{C}\}$. Let

$$\boldsymbol{X}_I(c) = \left\{\boldsymbol{x}_I^*(\boldsymbol{c}) \middle| \boldsymbol{x}_I^*(\boldsymbol{c}) \subset \boldsymbol{x}_I(\boldsymbol{c})\right\} - \emptyset$$

and

$$\boldsymbol{X}_I = \{\boldsymbol{X}_I(c) | c \in \boldsymbol{C}\}.$$

For $I = 14$ days, the best predictions were made in Miaoli with 100% accuracies for all predictions. The weighted accuracy probabilities over all counties are $P(\boldsymbol{x}_I) = 85.7\%$, $\overline{p}(\boldsymbol{x}_I) = 82.3\%$, and $p(\boldsymbol{x}_I) = 88.6\%$. In the remainder of this section we will consider the weighted average accuracies over all counties. Specifically, we investigate the impact of every measure $\boldsymbol{x}_{z,s,I} \in \boldsymbol{x}_{s,I}$ for $s \in \boldsymbol{S}$.

Define $\boldsymbol{x}_I(z,s) = \boldsymbol{x}_I - \{x_{z,s}\}$. By convention, $\boldsymbol{x_I = x_I}(\phi)$. Now, we simplify the notation as follows. Denote $P_{z,s}$ as $P(\boldsymbol{x}_I(z,s))$, $p_{z,s}$ as $p(\boldsymbol{x}_I(z,s))$, and $\overline{p}_{z,s}$ as $\overline{p}(\boldsymbol{x}_I(z,s))$. By convention, $P_\phi = P(\boldsymbol{x}_I)$, $\overline{p}_\phi = \overline{p}(\boldsymbol{x}_I)$, and $p_\phi = p(\boldsymbol{x}_I)$. The effects of each $x_{z,s}$ are elaborated as follows. Define the improvements of the above probabilities for $\boldsymbol{x}_I$ over $\boldsymbol{x}_I(x_{z,s})$ as

$$\upsilon_P(z,s) = \frac{P_\phi - P_{z,s}}{P_{z,s}} \quad \upsilon_{\overline{p}}(z,s) = \frac{\overline{p}_\phi - \overline{p}_{z,s}}{\overline{p}_{z,s}}$$

and

$$\upsilon_p(z,s) = \frac{p_\phi - p_{z,s}}{p_{z,s}}.$$

Table I shows the above prediction probabilities and improvements for 20 measure scenarios with $I = 14$ days, where the baseline is Scenario 1 using $\boldsymbol{x}_I$. Every scenario in this table is better than the scenario with $\boldsymbol{x}_I^*$ [21]. From this table, we have the following observations.

Scenarios 2–5 show the effects of BARP-I. Table I indicates that for any measure $\boldsymbol{x}_{z,B,I} \in \boldsymbol{x}_{B,I}$

$$-0.3\% \le \upsilon_P(z,B) \le 0.3\%. \tag{7}$$

By using the average and the day difference measures, the accuracy of net prediction is improved by 0.3%. By using the min, the max, or the range measures, the net prediction is

degraded by up to 0.3%. On the other hand, for the positive prediction

$$0.2\% \leq \upsilon_p(z, B) \leq 1.7\%. \tag{8}$$

Equation (8) indicates that the average, the min/max, and the range measures improve the positive prediction. The day difference measure slightly improves the positive prediction.

Scenarios 6–9 in Table I show the effects of Humidity-I. For any measure $\boldsymbol{x}_{z,H,I} \in \boldsymbol{x}_{H,I}$

$$-0.5\% \leq \upsilon_P(z, H) \leq 0.7\%. \tag{9}$$

The effects of the range and the day difference measures on the net prediction are not significant. The min/max measures have a more significant effect on improving the accuracy of net prediction. The average measure has a negative impact on the net prediction. From the description in Section II, it is clear that the change of relative humidity (and therefore the min and the max measures) is critical to the infection. The average value does not capture the humidity change and may be misleading. Therefore, the usage of the average measure is not recommended. The humidity measures have more impact on the positive prediction as shown in

$$-0.2\% \leq \upsilon_p(z, H) \leq 2.2\%. \tag{10}$$

Table I indicates that the min/max and the range measures significantly improve the accuracy of positive prediction and the average measure degrades the positive prediction.

Scenarios 10 and 11 show the effects of Rain-I. Table I indicates that for any measure $\boldsymbol{x}_{z,R,I} \in \boldsymbol{x}_{R,I}$

$$-0.2\% \leq \upsilon_P(z, R) \leq -0.1\%. \tag{11}$$

The information provided by Rain-I is already found in Humidity-I, which over compensates the humidity effect and has negative effects on the net prediction. On the other hand, for the positive prediction

$$0.7\% \leq \upsilon_p(z, R) \leq 1.2\%. \tag{12}$$

Equation (12) indicates that the Rain-I measures improve the accuracy of positive prediction.

Scenarios 12–15 in Table I show the effects of Temp-I. For any measure $\boldsymbol{x}_{z,T,I} \in \boldsymbol{x}_{T,I}$

$$-0.9\% \leq \upsilon_P(z, T) \leq 0.3\%. \tag{13}$$

The range measure has negative effect on net prediction. Other temperature measures improve the accuracy of net prediction. Equation (14) indicates that the Temp-I measures improve the accuracy of positive prediction, especially for the average measure

$$0\% \leq \upsilon_p(z, T) \leq 1.7\%. \tag{14}$$

Scenarios 16–19 show the effects of Spore-I. Table I indicates that for any measure $\boldsymbol{x}_{z,S,I} \in \boldsymbol{x}_{S,I}$

$$-0.5\% \leq \upsilon_P(z, S) \leq 0.3\%. \tag{15}$$

The average and the day difference measures for Spore-I improve the accuracy of net prediction, while the min/max and the range measures have negative effects on the net prediction. Equation (16) indicates that the Spore-I measures improve the accuracy of positive prediction. In particular, the effects of the range and the day difference measures are significant

$$0.4\% \leq \upsilon_p(z, S) \leq 1.2\%. \tag{16}$$

From (7)–(16), we observe that Rain-I does not have significant effect on net prediction. This may be due to the fact that its effect is already shown in Humidity-I. The effect of BARP-I is not very significant because this measure is seldom changed (see Fig. 6). Consider Scenario 20, a new scenario that excludes the measures causing negative $\boldsymbol{\upsilon_P}(z, s)$ in Table I, that is, the measure set $\boldsymbol{x_{I,20}}$ of this scenario is

$$\boldsymbol{x_{I,20}} = \boldsymbol{x_I} - \{x_{m,B,I}, x_{M,B,I}, x_{r,B,I}, x_{a,H,I}, x_{a,R,I}, x_{d,R,I} \\ x_{r,T,I}, , x_{m,S,I}, x_{M,S,I}, x_{d,S,I}\}.$$

We expect that Scenario 20 will yield the best net prediction performance. However, for $I = 14$, the AI model produces net prediction probability $P(\boldsymbol{x}_{14,20}) = 86.1\%$, negative prediction probability $\overline{p}(\boldsymbol{x}_{14,20}) = 83.4\%$, and positive prediction probability $p(\boldsymbol{x}_{14,20}) = 88.4\%$, which underperforms Scenario 14 for the accuracy probability of net prediction.

In Table I, the best net prediction occurs in Scenario 14 for $\boldsymbol{x}_I(r, T)$, and the best positive prediction occurs in Scenario 4 for $\boldsymbol{x}_I(a, H)$. Therefore, we try Scenario 21, a new scenario where $\boldsymbol{x}_{I,21} = \boldsymbol{x}_I(r, T) \cap \boldsymbol{x}_I(a, H)$. For $I = 14$, the resulting probabilities are $P(\boldsymbol{x}_{14,21}) = 86.3\%$, $\overline{p}(\boldsymbol{x}_{14,21}) = 83.1\%$, and $p(\boldsymbol{x}_{14,21}) = 89.2\%$. Clearly, Scenario 21 is better than Scenarios 1–20.

B. Effects of Threshold Spore-I and the Observation Period I

Instead of using (6), we may use the "threshold spore germination" function defined as

$$\delta(\, e_{T,i,n}\; e_{H,i,n}) = \begin{cases} 0, & \text{if } f_G(\, e_{T,i,n},\; e_{H,i,n}) < \theta \\ 1, & \text{otherwise} \end{cases} \tag{17}$$

where θ is the threshold such that if the probability of spore germination is higher than θ, then $\delta(\, e_{T,i,n}\; e_{H,i,n})$ predicts that rice blast occurs. Our experiments indicate that $\theta = 54\%$ is appropriate. Based on (17), we define a new measure for Spore-I in DataBank: the maximum value

$$\hat{x}_{M,S,i} = \max_{1 \leq n \leq N} \delta(i, n)$$

and $\boldsymbol{x}_{S,I}$ in (1) is replaced by

$$\widehat{\boldsymbol{x}}_{S,I} = \{\hat{x}_{M,S,i} | 1 \leq i \leq I\}.$$

By using the new spore measure, the $\boldsymbol{x}_I$ expression, i.e., (3) is replaced by

$$\widehat{\boldsymbol{x}}_{\boldsymbol{I}} = \boldsymbol{x}_{B,I} \cup \boldsymbol{x}_{H,I} \cup \boldsymbol{x}_{R,I} \cup \boldsymbol{x}_{T,I} \cup \widehat{\boldsymbol{x}}_{S,I}. \tag{18}$$

Now, we use the measure set $\widehat{\boldsymbol{x}}_I$ with threshold Spore-I in (18) for Scenario 22, a new scenario with

$$\boldsymbol{x}_{I,22} = \widehat{\boldsymbol{x}}_I - \{\boldsymbol{x}_{m,B,I}, \boldsymbol{x}_{M,B,I}, \boldsymbol{x}_{r,B,I}, \boldsymbol{x}_{a,H,I} \\ \boldsymbol{x}_{a,R,I}, \boldsymbol{x}_{d,R,I}, \boldsymbol{x}_{r,T,I}\}.$$

For $I = 14$, the resulting probabilities produced by Scenario 22 are $P(\boldsymbol{x}_{14,22}) = 87.2\%$, $\overline{p}(\boldsymbol{x}_{14,22}) = 85.6\%$, and $p(\boldsymbol{x}_{14,22}) = 89.1\%$, which can be considered better than Scenarios 1–21.

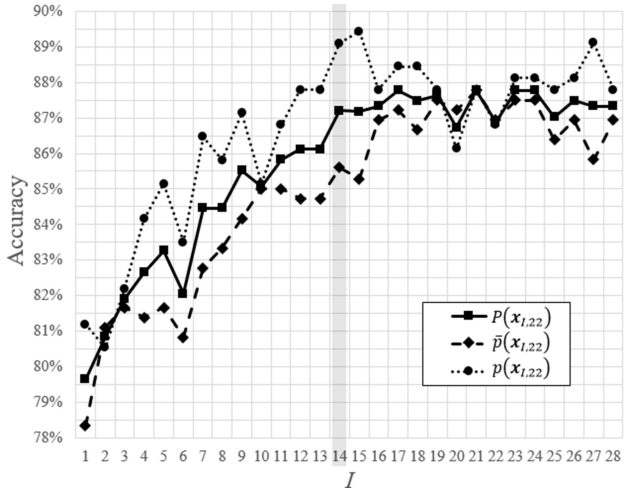

Fig. 11. Effects of I on $P(\boldsymbol{x}_{I,22})$, $p(\boldsymbol{x}_{I,22})$, and $\bar{p}(\boldsymbol{x}_{I,22})$.

The observation period I also has impact on the accuracies of prediction. Fig. 11 shows the trend that as I increases, the accuracy is improved. When $I > 15$ the improvement becomes insignificant. The best scenario occurs for $I = 15$, where $P(\boldsymbol{x}_{15,22}) = 87.2\%$, $\bar{p}(\boldsymbol{x}_{15,22}) = 85.3\%$, and $p(\boldsymbol{x}_{15,22}) = 89.4\%$, which has the same net prediction performance as the scenario where $I = 14$. Selecting 14 or 15 days as a period for CNN is reasonable because spore germination takes about two weeks [23]. While we try to optimize $p(\boldsymbol{x}_I(z, s))$, the false positive rate $1-\bar{p}[\boldsymbol{x}_I(z, s)]$ should be kept as low as possible. This section shows both good $p(\boldsymbol{x}_I(z, s))$ and $\bar{p}[\boldsymbol{x}_I(z, s)]$ in our approach. Therefore, we suggest to conduct the prediction using the scenario that yields the highest $p(\boldsymbol{x}_I(z, s))$.

VI. Conclusion

Based on the AgriTalk IoT platform for soil cultivation, we developed the RiceTalk application that utilizes nonimage IoT devices to detect rice blast disease. In our approach, the agriculture sensors generating nonimage data can be automatically trained and analyzed by the AI mechanism in real time. The beauty of RiceTalk is that the AI model is treated as an IoT device and therefore can be managed like other IoT devices. This approach nicely integrates AI into the IoT platform.

This article indicates that the min/max and the range measures for relative humidity and the average measure for temperature have significant effects on rice blast prediction. The average humidity measure may mislead the prediction especially when the variance (min/max) of humidity is large. The barometric pressure and rainfall do not significantly affect the net prediction results as compared with other weather measures. The rainfall effects are already covered by the humidity measures, and may not add much extra information for prediction. Barometric pressure is stable in one location, and therefore it is difficult to see its impact. However, both barometric pressure and rainfall do affect the positive prediction. In the future, we will investigate the effects of barometric pressure in multiple locations.

Spore germination is an important factor that causes rice blast. This factor has not been used for rice blast detection in the previous studies [10]. We have derived the spore germination prediction function that won a gold prize in the agricultural track in 2017 International Genetically Engineered Machine (iGEM) contest held by MIT. Details of this function are first reported in this article, and are subtly used as an extracted feature to improve the positive prediction of the CNN model from 87.1% to 89.4%, and improve the net prediction from 82.5% to 87.2%. From the view point of AI, this innovative spore germination mechanism is a new feature extraction model for agriculture.

Our experiments with different period lengths indicate that using weather data for every 14 or 15 days as a period is reasonable because spore germination takes about two weeks. By selecting appropriate measures for the RiceTalk AI model, we achieve 87.2% accuracy of the net prediction, and more importantly, 89.4% accuracy of the positive prediction.

References

[1] R. Dean *et al.*, "The top 10 fungal pathogens in molecular plant pathology," *Mol. Plant Pathol.*, vol. 13, no. 4, pp. 414–430, 2012.
[2] R. Bevitori and R. Ghini, "Rice blast disease in climate change times," *J. Rice Res.*, vol. 3, no. 1, pp. 1–2, 2014.
[3] *Bacterial Blight—IRRI Rice Knowledge Bank*. Accessed: Oct. 31, 2019. [Online]. Available: http://www.knowledgebank.irri.org/decision-tools/rice-doctor/rice-doctor-fact-sheets/item/bacterial-blight
[4] N. Petrellis, "A smart phone image processing application for plant disease diagnosis," in *Proc. 6th Int. Conf. Mod. Circuits Syst. Technol. (MOCAST)*, Thessaloniki, Greece, 2017, pp. 1–4.
[5] A. Ramcharan, K. Baranowski, P. McCloskey, B. Ahmed, J. Legg, and D. Hughes, "Using transfer learning for image-based cassava disease detection," in *Frontiers in Plant Science 8*. Ithaca, NY, USA: Cornell Univ., 2017, pp. 1–7.
[6] A. Johannes *et al.*, " Automatic plant disease diagnosis using mobile capture devices, applied on a wheat use case," *Comput. Electron. Agricult.*, vol. 138, pp. 200–209, Jun. 2017.
[7] K. Golhani, S. K. Balasundram, G. Vadamalai, and B. Pradhanc, "A review of neural networks in plant disease detection using hyperspectral data," *Inf. Process. Agricult.*, vol. 5, no. 3, pp. 354–371, 2018.
[8] W.-L. Chen *et al.*, "AgriTalk: IoT for precision soil farming of turmeric cultivation," *IEEE Internet Things J.*, vol. 6, no. 3, pp. 5209–5223, Jun. 2019, doi: 10.1109/JIOT.2019.2899128.
[9] J. M. Bonman, "Rice blast," in *Compendium of Rice Diseases*, R. K. Webster and P. S. Gunnel, Eds. St. Paul, MN, USA: Amer. Phytopathol. Soc. Press, 1992, pp. 14–18.
[10] D. Katsantonis, K. Kadoglidou, C. Dramalis, and P. Puigdollers, "Rice blast forecasting models and their practical value: A review," *Phytopathologia Mediterranea*, vol. 56, no. 2, pp. 187–216, 2017.
[11] M. A. K. Shafaullah, N. A. Khan, and Y. Mahmood, "Effect of epidemiological factors on the incidence of paddy blast (Pyricularia oryzae) disease," *Pakistan J. Phytopayhol.*, vol. 23, no. 2, pp. 108–111, 2011.
[12] Y. Li, W. Uddin, and J. E. Kaminski, "Effects of relative humidity on infection, colonization and conidiation of *Magnaporthe orzyae* on perennial ryegrass," *Plant Pathol.*, vol. 63, no. 3, pp. 590–597, 2014.
[13] L. S. Rajput, T. Sharma, P. Madhusudhan, and P. Sinha, "Effect of temperature on growth and sporulation of rice leaf blast pathogen *Magnaporthe oryzae*," *Int. J. Curr. Microbiol. Appl. Sci.*, vol. 6, no. 3, pp. 394–401, 2017.
[14] M. Saigusa, A. Yamamoto, and K. Shibuya, "Agricultural use of porous hydrated calcium silicate: Effect of porous hydrated calcium silicate on resistance of rice plant (Oryza sativa L.) to rice blast (Pyricularia oryzae)," *Plant Prod. Sci.*, vol. 3, no. 1, pp. 51–54, 2000.
[15] D. H. Long, F. N. Lee, and D. O. TeBeest, "Effect of nitrogen fertilization on disease progress of rice blast on susceptible and resistant cultivars," *Plant Disease*, vol. 84, no. 4, pp. 403–409, 2000.
[16] *CODiS, Observation Data Inquire System, Central Weather Bureau in Taiwan*. Accessed: Oct. 31, 2019. [Online]. Available: http://e-service.cwb.gov.tw/HistoryDataQuery/index.jsp

[17] Y.-W. Lin, Y.-B. Lin, and C.-Y. Liu, "AItalk: A tutorial to implement AI as IoT devices," *IET Netw.*, vol. 8, no. 3, pp. 195–202, May 2019, doi: 10.1049/iet-net.2018.5182.
[18] H. Hassouni, M. Ismaili-Alaoui, K. Lamrani, I. Gaime-Perraud, C. Augur, and S. Roussos, "Comparative spore germination of filamentous fungi on solid state fermentation under different culture conditions," *Micologia Aplicada Int.*, vol. 19, no. 1, pp. 7–14, 2007.
[19] J. R. Úrbez-Torres, E. Bruez, J. Hurtado, and W. D. Gubler, "Effect of temperature on conidial germination of Botryosphaeriaceae species infecting grapevines," *Plant Disease*, vol. 94, no. 12, pp. 1476–1484, 2010.
[20] L. H. Jacome, W. Schuh, and R. E. Stevenson, "Effect of temperature and relative humidity on germination and germ tube development of Mycosphaerella fijiensis var. difformis," *Phytopathology*, vol. 81, no. 12, pp. 1480–1485, 1991.
[21] W.-L. Chen *et al.*. *Disease Occurrence Model*. Accessed: Oct. 31, 2019. [Online]. Available: http://2017.igem.org/Team:NCTU_Formosa/Disease_Occurrence_Model
[22] D. P. Kingma and J. L. Ba, "Adam: A method for stochastic optimization," in *Proc. Int. Conf. Learn. Represent.*, 2015, pp. 1–15.
[23] R. J. Howard and B. Valent, "Breaking and entering: Host penetration by the fungal rice blast pathogen Magnaporthe grisea," *Annu. Rev. Microbiol.*, vol. 50, no. 1, pp. 491–512, 1996.
[24] A. Krizhevsky, I. Sutskever, and G. E. Hinton, "Imagenet classification with deep convolutional neural networks," in *Proc. Adv. Neural Inf. Process. Syst.*, 2012, pp. 1097–1105.
[25] G. E. Hinton, N. Srivastava, A. Krizhevsky, I. Sutskever, and R. R. Salakhutdinov, "Improving neural networks by preventing co-adaptation of feature detectors," *arXiv preprint arXiv:1207.0580*, 2012.

Wen-Liang Chen received the Ph.D. degree in biotechnology from National Chiao Tung University, Hsinchu, Taiwan, in 2006.

He joined National Chiao Tung University in 2008, where he is an Associate Professor with the Department of Biological Science and Technology. His current research interests include protein chemistry, protein engineering, synthetic biology, cancer biology, antibody engineering and development of biomaterial-based drug repositioning platforms for cancer treatment.

Yi-Bing Lin (M'96–SM'96–F'03) received the bachelor's degree from National Cheng Kung University, Tainan, Taiwan, in 1983, and the Ph.D. degree from the University of Washington, Seattle, WA, USA, in 1990.

From 1990 to 1995 he was a Research Scientist with Bellcore (Telcordia), Piscataway, NJ, USA. He is the Winbond Chair Professor with National Chiao Tung University (NCTU), Hsinchu, Taiwan, where he became a Lifetime Chair Professor in 2010 and the Vice President in 2011. From 2014 to 2016, he was a Deputy Minister with the Ministry of Science and Technology, Taipei, Taiwan. Since 2016, he has been appointed as a Vice Chancellor with the University System of Taiwan (for NCTU, NTHU, NCU, and NYM).

Prof. Lin is a fellow of AAAS, ACM, and IET.

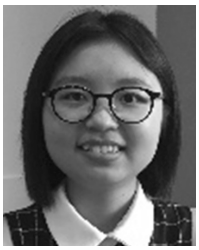

Fung-Ling Ng received the B.S. degree in biological science and technology from National Chiao Tung University, Hsinchu, Taiwan, in 2017, where she is currently pursuing the Ph.D. degree.

Her current research interests include biopesticides application and precision farming management.

Chun-You Liu received the B.S. degree in mathematics from National Taiwan University, Taipei, Taiwan, in 2012, where he is currently pursuing the Ph.D. degree in computer science.

Since 2013, he has been with the Industrial Technology Research Institute, National Chiao Tung University, Hsinchu, Taiwan, where he is a Researcher and an Engineer with the Computational Intelligence Technology Center. His current research interests include machine learning, deep reinforcement learning on robotic applications, computer vision, pattern recognition, prognostics and health management, abnormal detection, convolutional neural networks, and deep neural networks.

Mr. Liu was a recipient of the 2017 Research and Development 100 Awards. He is a member of Phi Tau Phi Scholastic Honor Society.

Yun-Wei Lin received the Ph.D. degree in computer science and information engineering from National Chung Cheng University, Chiayi, Taiwan, in 2011.

He has been an Assistant Professor with the College of Artificial Intelligence, National Chiao Tung University, Hsinchu, Taiwan since 2019. His current research interests include mobile ad hoc network, wireless sensor network, vehicular ad hoc networks, and Internet of Things/M2M communications.